EUROPEAN ROTORCRAFT FORUM 2017: 718

DESIGN AND MANUFACTURE OF INSTRUMENTED ROTOR BLADES FOR A HELICOPTER TEST RIG

Samuel Furtado[1], Antonio Filippone[2] & Nicholas Bojdo[2], Constantinos Soutis[1, 3]

[1]School of Materials,
[2]School of Mechanical, Aerospace and Civil Engineering,
[3]Aerospace Research Institute,
University of Manchester, Manchester M13 9PL, UK.

Abstract

Rotor blades have been designed, optimised, and manufactured for a national wind tunnel facility in the UK. The design included constraints such as blade diameter, to fit into existing wind tunnels, prescribed maximum centrifugal loads, and a unique fully articulated rotor head, capable of operating both as a conventional rotor and as a tilt-rotor. Two rotors having four instrumented blades each were finally produced. The rotors are mounted on a common rotor head on a rig, with or without rotorcraft fuselages. With the rotor head and hinges designed independently, important structural constraints were imposed on the overall blade design and aerodynamic loads. The Mach number scaled profiles were expected to generate 2.5 KN (at 2,500 rpm) and 3kN (at 3,000 rpm) of thrust for the helicopter and the tilt rotor blades, respectively. The maximum permissible radial hub load was 15kN. The embedded instrumentation was used to capture the blades vibration modes. The use of carbon fibre composites enabled a successful design and manufacturing of instrumented blades.

Keywords: rotorcraft blades design; blades manufacturing; blades instrumentation; composite materials; wind tunnel testing.

1. INTRODUCTION

Helicopters present several advantages when compared with fixed wing aircraft, most notably vertical take-off and landing, making them the only viable means of transportation in many applications where space is limited. Their use ranges from rapid urban transportation to rescue and military missions. They are very complex and unique machines requiring broad and deep engineering knowledge for proper design and manufacturing. Analytical models to design and predict their performance have been extensively studied, allowing some great innovations to be introduced [1, 2]. Meanwhile, problems like noise and vibration still persist. These are due to the number of components and their complexity involved. In order to improve the models, wind tunnel testing results have proved to be an important tool. Here, scaled or full-scale prototypes can be tested in replicated real flight conditions [3, 4].

In this project, a wind tunnel rotor rig capable for scaled helicopter and tilt rotor blades testing was designed and manufactured. The objective was to increase the capability to better understand the phenomenon regarding rotorcraft performance. This will contribute to improving models, making the design process more efficient and expedite.

The design and manufacturing of a set of blades to test the rotor rig capabilities was the main task of the current project. The design included constraints such as blade diameter, to fit into existing wind tunnels, prescribed maximum centrifugal loads, and a unique fully articulated rotor head, capable of operating both as a conventional rotor and as a tilt-rotor. Two rotors having four instrumented blades each were finally produced. The rotors are mounted on a common rotor head on a rig, with or without the rotorcraft fuselage. This paper discusses the steps and challenges considered during the development of the advanced composite blades.

2. BLADE DESIGN

2.1 Aerodynamic-Structural Design

The aerodynamic design was constrained by the wind tunnel capability (dimensions of the test section and wind speed) and by the rotor head design loads. Thus, the overall dimensions are specified by the available space and the mass distribution is constrained by the centrifugal loads at the design point. The rotors are Mach-scaled. Another constraint is the design thrust, which was required to not exceed 3 kN. The final geometry is given by a trim condition of zero net thrust. Both rotors are four-bladed, and are mounted on an articulated rotor head and gear-box that can swivel to produce tilt-rotor inflow conditions. The

rotor blades have a diameter of 1.80 m, with a design angular speed of 2,300 rpm, and the tilt-rotor blades have a diameter of 1.40 m, with a design angular speed of 3,000 rpm. The design parameters for the tilt-rotor and helicopter blades are summarised in Table 1 and Table 2.

Blades	4
Design diameter	1.800 m
Blade chord (constant)	0.071 m
Solidity ratio	0.0497
Effective blade span	0.514 m
Blade twist, linear	9.97 degrees
Design speed	2,300 rpm
Design tip Mach number	0.644
Pre-cone angle	0.0 degrees

Table 1: Helicopter blade design parameters

Blades	4
Design diameter	1.400 m
Blade chord, root	0.082 m
Solidity ratio	0.01418
Effective blade span	0.514 m
Blade volume	495.45 cm^3
Blade twist, non linear	17.91 degrees
Design speed	3,000 rpm
Design tip Mach number	0.646
Pre-cone angle	0.0 degrees

Table 2: Tilt-rotor blade design parameters

Three reference sections were set for the tilt-rotor: Boeing-Vertol V23010-1.58 (10% thick) for the outer section; a Vertol V43015-2.48 (15%) thick for the mid-section and a non-standard NACA 64128 aerofoil (28%) at the root. All these aerofoil sections had to be modified. The geometrical design involved additional control points, surface smoothing, constraint on relative thickness and opening of the trailing edge gap to provide a finite-thickness trailing-edge that could be manufactured.

The design was carried out by using a combined blade-element and momentum theory computer code, which included a transonic aerodynamic model and an iterative trim condition. In this specific instance, the net thrust was the constraint and the configuration was adjusted to the specified thrust, for example zero or limit value. The key requirement that constrained the blade mass and moment of inertia was the maximum permissible radial hub load, which was set at 15 kN. A constraint chart was constructed, based on a simple dynamic relationship between the rotor blade mass, radius of gyration and centrifugal load. From this analysis, consider a blade of mass 450g. The maximum permissible radius of gyration would be 0.338m (or r/R = 0.48 for blade of 0.7m span). This leads to a maximum permissible moment of inertia of 0.051 kgm^2. The moment of inertia constraint is sensitive to the total mass of the blade, Figure 1; after each design iteration of internal structural layout of the blade, a quick conformity check of the 'new' moment of inertia at the new blade could be facilitated by the use of the constraint diagram in Figure 1. This was a useful tool as the blade design went through many changes in the design of the root attachment. The same process was also followed for the helicopter blades (Figure 2).

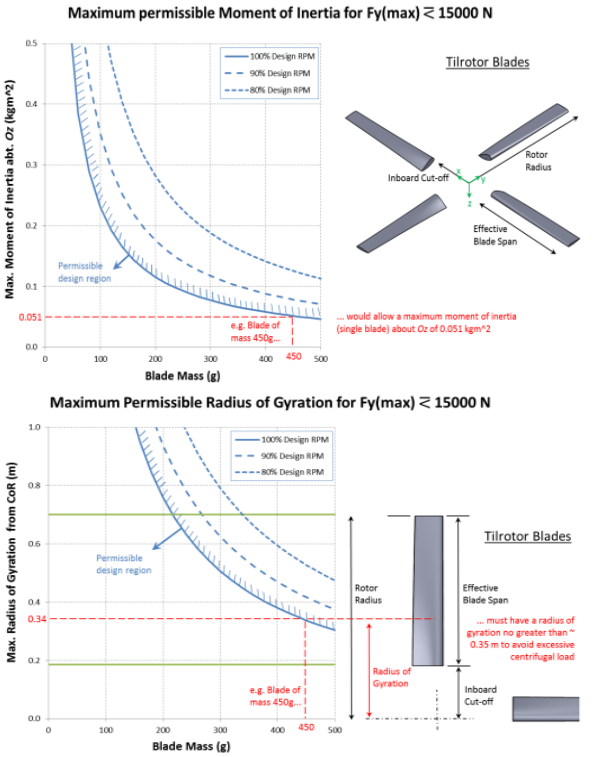

Figure 1: Constraints chart of centrifugal force and radius limit for initial design of tilt rotor blades.

Using the lumped mass approximation, an initial 'target' weight was established. Then, by using finite element analysis software, analysis was performed to determine failure. The design was also changed in order to reduce the blade deflections. After several iterations, the optimized solutions presented in the **Error! Reference source not found.** were achieved.

For the tilt rotor blades, the solution consisted of a composite aerofoil skin, a D-spar, an aluminium metal root fitting. The D-spar was made of a composite skin and a foam core to increase the blade stiffness without compromising the weight. To increase the tear/bearing strength in the aluminium root fitting where shear pin is connected, *collar rings* (maraging steel) are considered.

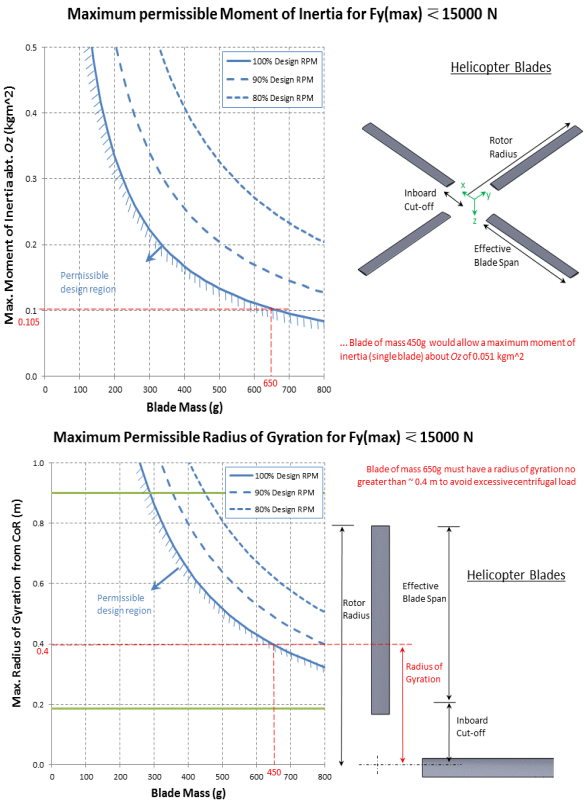

Figure 2: Constraints chart of centrifugal force and radius limit for initial design of helicopter blades.

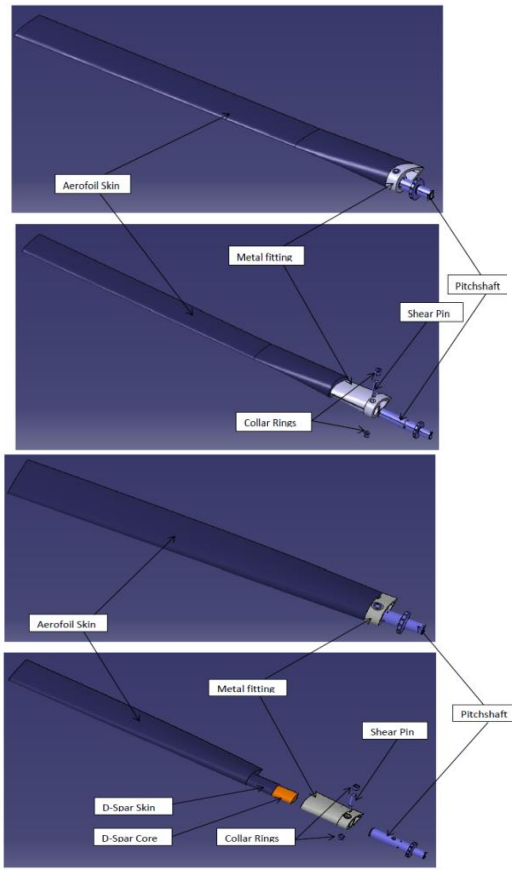

Figure 3: Blades design solutions: a) helicopter (top two); b) tilt rotor (bottom two).

The helicopter blade solution was similar to the tilt rotor one, apart from the absence of a D-spar: a composite aerofoil skin and an aluminium metal root fitting. In this case, the thinner aerofoil cross-section, made the use of a D-spar impractical. To overcome this constraint, changes in the composite skin lay-up were considered, where different ply orientation and higher number of plies were selected.

The requirement for internal instrumentation determines that blades have to be manufactured in two separate halves and bonded together after the instrumentation has been installed.

2.2 Finite-element Analysis

The FEA was performed using ABAQUS software. The mechanical properties were provided by the materials suppliers and used during the FEA for the tilt rotor and for the helicopter blades. Centrifugal, thrust and drag forces were applied. For the centrifugal force, the helicopter and tilt rotor blades are considered rotating at constant speed of 2400 rpm and 3000 rpm, respectively. The four helicopter blades are expected to generate 2.5 KN and the four tilt rotor ones 3kN. The thrust and drag loads are applied as a point load span wise in the aerofoil in accordance to the aerodynamic predictions at the corresponding cross-section ¼ chord (Figure 3 and Figure 4).

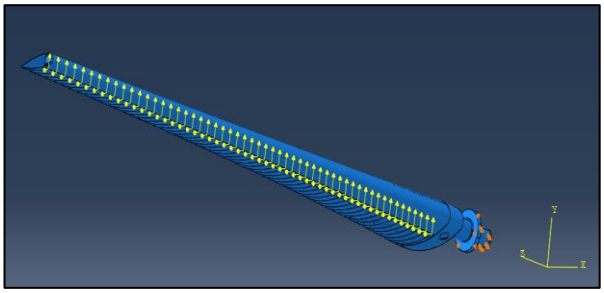

Figure 3: Tilt rotor thrust and drag loads: ¼ cord application during FEA.

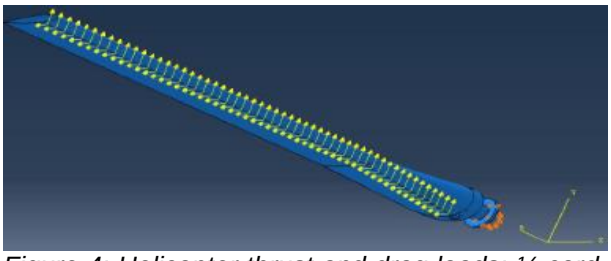

Figure 4: Helicopter thrust and drag loads: ¼ cord application during FEA.

The reaction of the centrifugal force is considered to be at thrust bearing of the rotor head, for this reason the displacement u_z of the pitch shaft where there the contact with the thrust bearing

occurs is considered to be zero. The roller bearing constrains the movements in the other two directions, u_x and u_y.

2.2.1 Tilt rotor blades results

The FEA results for the tilt rotor blade are summarised in the **Error! Reference source not found.**.

Mass	354	g
CoG (z)	327.8	mm
Iyy (CoG)	8.900	$Mg.mm^2$
Izz	0.047	$Mg.mm^2$
Radius of gyration	364.2	mm
Max radial force, R_F	13.7	kN
Max deflection, δ_y	19.8	mm
Max distortion, θ_z	0.86	deg

Table 3: FEA results for tilt rotor blades.

The design solution considered (**Error! Reference source not found.**) expects a blade mass of 354g and centrifugal force (R_F) of 13.7kN. Considering the I_{zz} and radius of gyration, the results are in accordance with the value predicted by the lumped mass approximation (Figure 5), ensuring a centrifugal force below the maximum allowed 15kN.

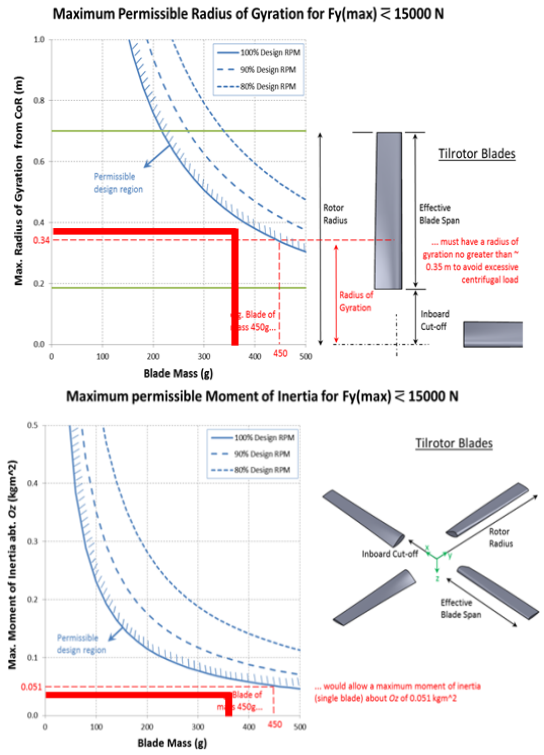

Figure 5: Comparison of the tilt rotor blade results with the relation between mass distribution and centrifugal forces (achieved values in solid red).

It is expected that the maximum deflection (δ_y) and distortion (θ_z) to be 19.80 mm and 0.86°, respectively.

Due to the presence of a flap hinge in the rotor head, the blades, during their normal working conditions, are not expected to experience the maximum thrust value reaction. However, in the presence of a problem in the flap hinge, this could mean that the maximum thrust will be experienced by the blades, resulting in higher stresses in the blades. Therefore, the blades will be performing between a condition where they will experience only the effects of the centrifugal loads and where they will experience both the centrifugal loads and thrust loads.

2.2.2 Helicopter blades results

The FEA results for the helicopter blade are presented in the Table 3.

Mass	415	g
CoG (z)	20.9	mm
Iyy (CoG)	20.900	$Mg.mm^2$
Izz	0.078	$Mg.mm^2$
Radius of gyration	433.0	mm
Max radial force, R_F	10.2	kN
Max deflection, δ_y	53.7	mm
Max distortion, θ_z	4.09	deg
Tsai-hill (aerofoil)	0.27(L5)	-

Table 3: FEA results for helicopter blades.

The results show that reaction force (centrifugal force), R_F in the thrust bearing is clearly below the maximum allowed value (15kN). For the expected mass (415g), this is in accordance with the value predicted by the lumped mass approximation (Figure 6).

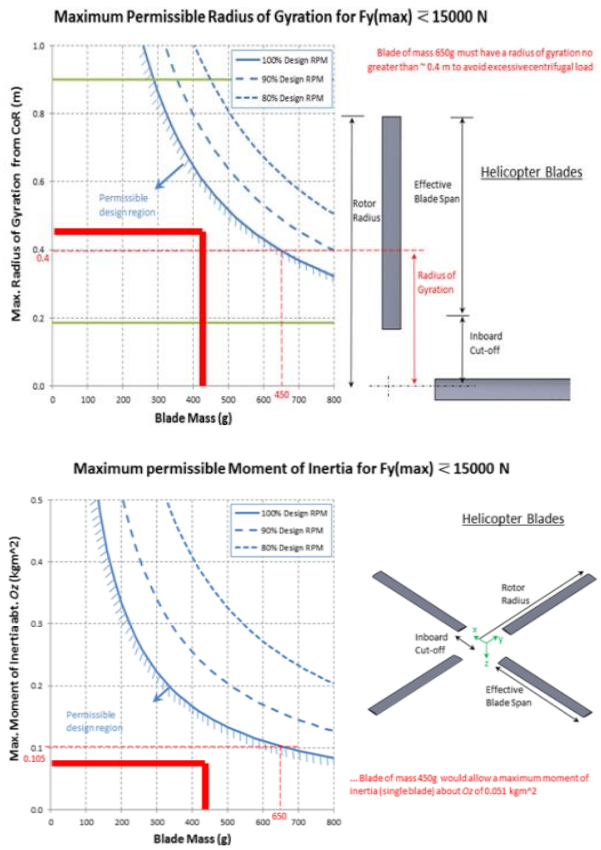

Figure 6: Comparison of the helicopter blade results with the relation between mass distribution and centrifugal forces.

The blade deformation is presented in Figure 7. The tip maximum deflection (δ_y) is 52.70 mm and the maximum distortion (θ_z) is 4.09°.

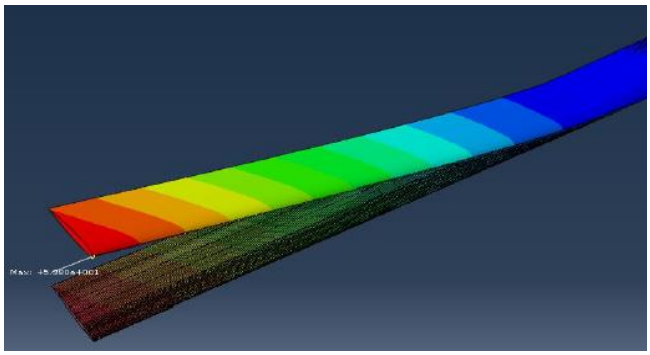

Figure 7: Helicopter blade deflection result.

It can be noticed that in the aerofoil skin where a severe cross-section transition occurs, stress concentration effects are noticed (Figure 8). This severe cross-section transition was necessary in order to facilitate the root fitting design and posterior assembly.

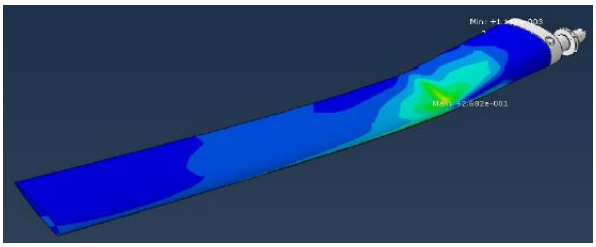

Figure 8: Helicopter blade von Mises result, showing the stress concentration effects.

Similarly to the tilt rotor blade, the two flap hinge conditions are also considered - only the effects of the centrifugal loads, and both the centrifugal loads and thrust loads effects.

3. TOOLING & MANUFACTURE

It is understood that after each blade set is manufactured, there may be small weight values and distribution differences between the blades. This potential difference in weigh value and distribution will induce additional loads and vibrations affecting the rotor rig stability, control and safety [5]. Therefore, the blade set balancing is a critical aspect that has to be considered.

To ensure that the blades are balanced, a solution that allows mass to be added/located at different locations was determined for both blade sets. The solution consists of a composite tip-cap that will be attached at the blade tip (Figure 9). The tip-cap has a composite skin and aluminium core. The cap will have a shape that will ensure a perfect match with the blade, ensuring that no extra interference in the aerofoil occurs. Two external layers of the same pre-peg considered in the manufacturing of the aerofoil skin and an aluminium core is used. The use of the aluminium core allows the use of screws as balancing mass. In each blade set an array of tapered holes is considered, and the holes will be used in accordance with the balancing needs. This solution of composite and aluminium will also ensure low level of weight, which is very important at greater radius (e.g. tip) to keep the centrifugal forces low.

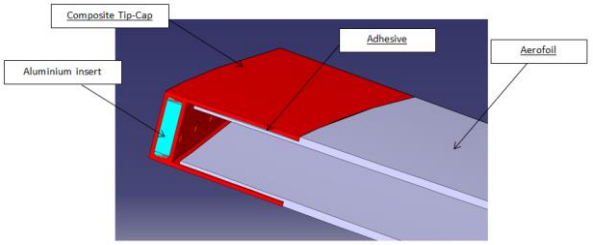

Figure 9: Balancing solution for tilt rotor blade and helicopter blade sets.

The composite parts (aerofoil skin, D-spar and tip-cap) were manufactured using carbon-epoxy prepreg cured in an autoclave. The final mould solution for the aerofoil skin and tip-cap was CNC machined in an aluminium block to allow higher temperatures (130°C), and therefore shorter curing cycle time.

An in-house automated ply-cutter machine was used to cut the prepreg layer in the require orientation and shape. This ensures more accuracy and consistency within the blades. Then, the plies were laid-up in accordance with the desired stacking sequence, and vacuum bag were prepared to be cured in the Autoclave. Figure 10 presents pictures of half skins for the two blade sets, helicopter and tilt rotor blades.

Figure 10. Helicopter and tilt rotor blade skins manufactured.

Regarding to the tip-caps, the core was cut using in-house water-jet machine. The plies were laid-up, and vacuum bag was prepared, and then cured in the Autoclave.

The tilt rotor D-Spar core CAD model was generated from the aerofoil design and use to CNC machine foam (Figure 11 left). After, prepreg plies were laid-up to create the required laminate. The laminate were “vacuum bagged” using aerofoil skin mould as jig, ensuring every part will have the same established profile shape (Figure 11, bottom).

Figure 11. Tilt rotor blade D-Spar. Top: Core; Bottom: D-Spar manufactured.

After manufacturing of the composite parts, they were trimmed. In order to have similar mass within the blade sets, complementary skin halves were combined to ensure smallest possible differences between four blades in each set. Then, electrical strain gauges and wires were carefully aligned and bonded to the skins.

The assembly process followed. Adhesive was used to connect the parts. First, the half skins were assembled. For the tilt rotor blades, the D-spar was also assembled during this stage. In the case of the skin halves, a solution of co-curing the adhesive and prepreg was considered. The co-curing solution has proved to be an efficient method to join composite parts and components [6]. The idea is to cure the composite plies and the adhesive ply at the same time, improving the adhesion and reducing production times. Here, an additional aspect was explored. Since the surface area for bonding is only the thickness of the composite skin a strip of the prepreg was used as media to connect the two half skins. This means the load transfer between the half skins through the prepreg layer. Therefore, the combination of the adhesion property of the adhesive and the stiffness/strength properties of the prepreg were achieved.

For the co-curing process, the surfaces were de-greased and de-contaminated, and the bonding mediums (adhesive + prepreg) were placed in its correct location (Figure 12 left).

To ensure the similar shape within each blade set, the corresponding mould was used as an assembly jig. The half skin moulds were made in a way that, when closed, to be possible to obtain the required aerofoil profile. After, internal vacuum bagging was done, which ensures the required curing pressure is uniformly distributed (Figure 12 right).

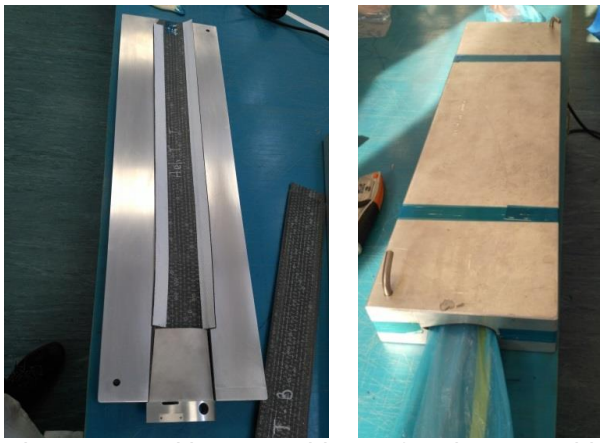

Figure 12. Skin assembly. Left: close mould; centre: prepreg + adhesive strips placement; right: vacuum bagging.

After the half skin assembly, the root fittings were attached. The fitting bonded surface area was sandblasted to create the require roughness. Then, surface was de-greased and de-contaminated before placing the adhesive. The fitting with the adhesive was then inserted into the skin. The assembly was placed in a vacuum bag, and the sets were cured under the conditions recommended by the adhesive supplier. A similar procedure was carried-out for the tip-caps assembly.

3.1 Blade Instrumentation

The main objective for the instrumentation is to enable identification of the blade's vibrational modes. Additionally, to avoid any interference on the aerodynamic performance, the instrumentation had to be internal. Studies have shown that electrical strain gauge can successfully be used to characterise the vibrational behaviour of components [7]. By capturing the strain at specific locations, the natural frequencies and mode shapes can be determined. This will characterise the vibrational behaviour of the blades when connected to the rotor rig head.

Using the FEA software, the vibrational mode shapes were identified and suitable locations for strain gauge placement were estimated. The number and the locations of the strain gauges must ensure a unique strain measurement pattern. This means that combining the strain measurements in a specific natural mode in each point will be characteristic of only that mode shape. Therefore, this will differentiate each mode. The Figure 13 shows some modes obtained by FEA for the tilt rotor blades.

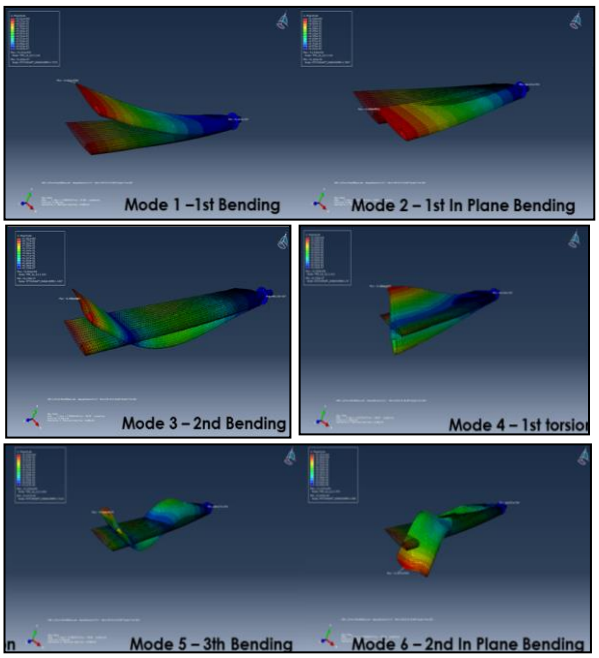

Figure 13: Tilt rotor blade vibrational modes.

The first 3 bending, 2 lead lag (in-plane) bending and 2 torsion modes are identified. In this case, it was noticed that it is required four points (locations) to identify the 3 bending. For the first 2 lead lag bending and torsion modes three locations are required. Therefore, a total of 10 locations are determined. The strain that characterise the bending modes (flap and lead lag) is axial in the spanwise direction. Meanwhile, the torsion ones are characterised by the shear strain.

To amplify the reading signal the full-bridge connection was considered. The full-bridge connection requires the use of four strain gauges to measure the strain at a specific location. These strain gauges should be placed relatively close to each other that the reading will be the sum of the absolute value of these four strain measurements.

3.1.1 Tilt rotor blades

The first 10 modes were identified using the FEA and presented in Table 4. The corresponding natural frequencies, considering and not considering the rotor head rotation, are also presented. It can be noticed that the rotor head

rotation increases the natural frequency of the tilt rotor blade, as expected.

Modes	Natural Frequency [Hz]		Mode Type
	With Rotation	Without rotation	
1	112.61	89.56	Flap Bending
2	156.00	118.21	Lag Bending
3	401.00	372.02	Flap Bending
4	721.01	718.8	Torsion
5	812.98	787.2	Flap Bending
6	991.41	984.51	Lag Bending
7	1226.40	1184.5	Flap Bending
8	1326.40	1292.5	Torsion
9	1471.70	1414.1	Lag Bending
10	1657.90	1594.5	Torsion

Table 4: Natural frequencies and vibration modes for tilt rotor blades.

The location of the reading points are presented in Figure 14.

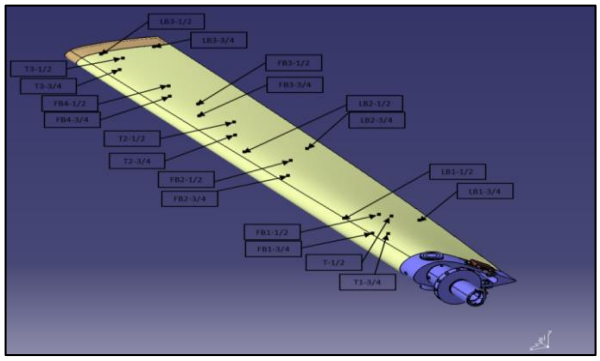

Figure 14: Location of strain measurement points for tilt rotor blade.

3.1.2 Helicopter blades

Table 5 presents the first 10 mode shapes identified using the FEA for the helicopter blades.

Modes	Frequencies [Hz]		Type
	With Rotation	Without rotation	
1	60.64	31.88	Flap Bending
2	95.23	74.09	Lag Bending
3	209.85	173.83	Flap Bending
4	362.15	392.42	Torsion
5	443.44	401.70	Flap Bending
6	553.68	524.65	Lag Bending
7	679.53	627.27	Flap Bending
8	919.33	861.17	Flap Bending
9	1004.10	984.89	Torsion
10	1145.00	1084.00	--------

Table 5: Natural frequencies and mode shapes for the model helicopter blade.

The natural frequencies, considering and not considering the rotor head rotation, are also presented. Similarly to the tilt rotor case, the rotor head rotation increases the natural frequency of the tilt rotor blade.

The location of the strain reading points are presented in Figure 15.

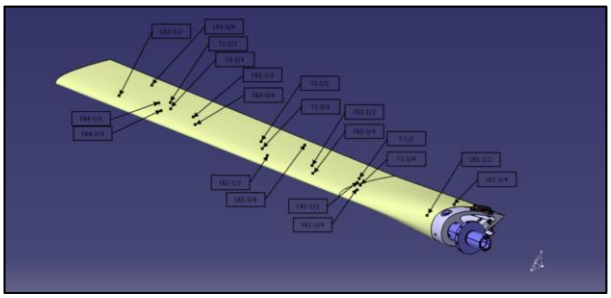

Figure 15: Location of strain measurement points for helicopter blade.

Afterwards, the strain gauges were bonded on determined locations for each half skins. The electrical wires were bonded to the skins surface to ensure that they will not be loose while the blades are rotating. The wire bonding followed the same pattern for each half skin, ensuring the same weight distribution within each blade set (Figure 16).

Figure 16: Wire bonding. Top: Helicopter blades; Bottom: Tilt rotor blades.

4. CONCLUSIONS

The use of composite materials, enabled a successful design and manufacturing of instrumented blades, where the weight requirement was fulfilled and allowing the wind tunnel constraints to be met. The composite materials also provided bigger design flexibility, enabling the designer to 'tailor' some material properties in accordance with the requirement. However, the manufacturing and instrumentation present several challenges, especially due to small sizes encountered in this study. Special tools and equipment may be required for trimming and assembling. The lumped mass approximation revealed as a very useful tool during the design optimisation iterations, where from the blade mass, moment of inertia and radius of gyration values, the expected centrifugal forces can easily be determined.

ACKNOWLEDGMENTS

The research presented in this paper was part of the UK National Rotor Rig Facility. The authors thank the Aerodynamic Research Association (ARA) and the UK Aerospace Techology Institute for their financial support.

REFERENCES

1. Keener, J.K., *The helicopter innovation in Army aviation.* 2001.
2. Brocklehurst, A. and G.N. Barakos, *A review of helicopter rotor blade tip shapes.* Progress in Aerospace Sciences, 2013. **56**: p. 35-74.
3. Norman, T.R., et al., *Full-scale wind tunnel test of the UH-60A airloads rotor*. 2011, Army Research Development And Engineering Command Moffett Field Ca Aviation Aeroflight Dynamics Directorate.
4. Bao, J., et al., *Wind Tunnel Test of Five Sets of Mach Scale Composite Tailored Rotor with Flap-Bending/Torsion Couplings for Vibration Reduction.* Journal of the american helicopter society, 2008. **53**(3): p. 215-225.
5. Kunz, D.L. and M.C. Newkirk, *A generalized dynamic balancing procedure for the AH-64 tail rotor.* Journal of Sound and Vibration, 2009. **326**(1): p. 353-366.
6. Shin, K.C., J.O. Lim, and J.J. Lee, *The manufacturing process of co-cured single and double lap joints and evaluation of the load-bearing capacities of co-cured joints.* Journal of Materials Processing Technology, 2003. **138**(1): p. 89-96.
7. Hillary, B. and D.J. Ewins. *The use of strain gauges in force determination and frequency response function measurements*.